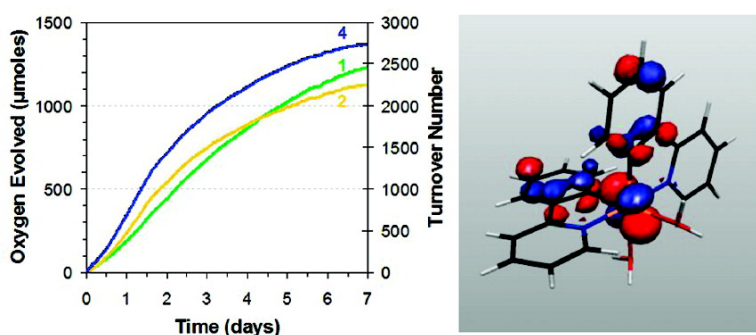**Article**

Cyclometalated Iridium(III) Aquo Complexes: Efficient and Tunable Catalysts for the Homogeneous Oxidation of Water

Neal D. McDaniel, Frederick J. Coughlin, Leonard L. Tinker, and Stefan Bernhard

More About This Article

Additional resources and features associated with this article are available within the HTML version:

- Supporting Information
- Links to the 14 articles that cite this article, as of the time of this article download
- Access to high resolution figures
- Links to articles and content related to this article
- Copyright permission to reproduce figures and/or text from this article

View the Full Text HTML

Cyclometalated Iridium(III) Aquo Complexes: Efficient and Tunable Catalysts for the Homogeneous Oxidation of Water

Neal D. McDaniel, Frederick J. Coughlin, Leonard L. Tinker, and Stefan Bernhard*

Contribution from the Department of Chemistry, Princeton University, Princeton, New Jersey 08544

Received June 19, 2007; E-mail: bern@princeton.edu

Abstract: A series of bis-phenylpyridine, bis-aquo iridium(III) complexes is herein shown to robustly and efficiently catalyze the oxidation of water to dioxygen in the presence of a sacrificial oxidant. Through substitution on the cyclometalating ligands of these complexes, it is shown that a broad range of oxidation potentials can be achieved within this class of catalyst. Parallel, dynamic monitoring of oxygen evolution, made possible by equipping reaction vessels with pressure-voltage transducers, facilitates correlation of these complexes' ionization potentials with their respective activity toward water oxidation. The importance of these catalysts lies in (A) their ability to oxidize water in a purely aqueous medium, (B) their simplicity of design, (C) their durability, and (D) the ease with which they can be tuned to accommodate the electrochemical needs of photosensitizers in hypothetical photochemical water oxidation and full artificial photosynthetic schemes.

Introduction

Anticipation of increased global energy consumption has fostered widespread desire to efficiently collect and store solar energy in the form of dihydrogen and other fuels. Artificial photosynthesis is one strategy for accomplishing this task. In short, it is the goal of photosynthetic systems to photolytically convert a common redox product (in this case water) into its fuel and oxidant parent materials (H_2 and O_2), thereby storing solar energy for later use. The development of a good artificial photosynthetic system represents a complex challenge that becomes more practicable when divided into its photophysical and electrochemical components. The electrochemical aspect of this endeavor is typically further broken down into its oxidative and reductive half-reactions, which can be studied independently. While much progress has been made in the field of water reduction to evolve dihydrogen gas, the complementary oxidative half-reaction has proven far more difficult to achieve.[1−4] The challenge of water oxidation primarily lies in the implicit complexity of mediating four highly energetic charge transfers to catalytically obtain only the desired dioxygen product, despite the reaction's harshly oxidative environment.

The first step in homogeneous, photodriven water oxidation is activation of the oxidation catalyst through interaction with the energetic, oxidized state of a photosensitizer molecule, such as $[Ru(bpy)_3]^{3+}$ or $[Ir(ppy)_2(bpy)]^{2+}$ (bpy = 2,2′-bipyridine, ppy = 2-phenylpyridine). However, to avoid complications like photosensitizer decomposition, a single-electron, sacrificial oxidant is typically employed in place of the photosensitizer to

facilitate direct investigation of the catalyst. By far the most widely used oxidant for this purpose is the ceric ion, which, despite its 1.72 volt oxidative potential vs NHE, is only capable of oxidizing water very slowly under intense irradiation.[5]

Previously reported water oxidation catalysts for homogeneous and microheterogenous water splitting systems generally fall into two categories. First, there is the oxo- and otherwise bridged, bi-, and multinuclear transition metal complex system, first pioneered by Meyer et al. in the early 1980s.[6−22] Additionally, there is a body of work that deals with turning metal oxides with moderate band gaps into colloidal suspensions of nanoscopic electrodes.[23−29] Of particular interest to the current work

(1) Meyer, T. J. *Acc. Chem. Res.* **1989**, *22*, 163−170.
(2) Rüttinger, W.; Dismukes, G. C. *Chem. Rev.* **1997**, *97*, 1−24.
(3) Hurst, J. K. *Coord. Chem. Rev.* **2005**, *249*, 313−328.
(4) Alstrum-Acevedo, J. H.; Brennaman, M. K.; Meyer, T. J. *Inorg. Chem.* **2005**, *44*, 6802−6826.
(5) Evans, M. G.; Uri, N. *Nature* **1950**, *4223*, 602−603.
(6) Gersten, S. W.; Samuels, G. J.; Meyer, T. J. *J. Am. Chem. Soc.* **1982**, *104*, 4029−4030.
(7) Gilbert, J. A.; Eggleston, D. S.; Murphy, W. R., Jr.; Geselowitz, D. A.; Gersten, S. W.; Meyer, T. J. *J. Am. Chem. Soc.* **1985**, *107*, 3855−3864.
(8) Gilbert, J. A.; Geselowitz, D. A.; Meyer, T. J. *J. Am. Chem. Soc.* **1986**, *108*, 1493−1501.
(9) Ramaraj, R.; Kira, A.; Kaneko, M. *Angew. Chem.* **1986**, *98*, 824−825.
(10) Rotzinger, F. P.; Munavalli, S.; Comte, P.; Hurst, J. K.; Grätzel, M.; Pern, F.; Frank, A. J. *J. Am. Chem. Soc.* **1987**, *109*, 6619−6626.
(11) Wiedghardt, K. *Angew. Chem.* **1989**, *101*, 1179−1198.
(12) Yagi, M.; Tokita, S.; Nagoshi, K.; Ogino, I.; Kaneko, M. *J. Chem. Soc., Faraday Trans.* **1996**, *92*, 2457.
(13) Chronister, C. W.; Binstead, R. A.; Ni, J.; Meyer, T. J. *Inorg. Chem.* **1997**, *36*, 3814−3815.
(14) Limburg, J.; Brudvig, G. W.; Crabtree, R. H. *J. Am. Chem. Soc.* **1997**, *119*, 2761−2762.
(15) Lebeau, E. L.; Adeyemi, S, A.; Meyer, T. J. *Inorg. Chem.* **1998**, *37*, 6476−6484.
(16) Wada, T.; Tsuge, K.; Tanaka, K. *Inorg. Chem.* **2001**, *40*, 329−337.
(17) Sens, C.; Romero, I.; Rodriguez, M.; Llobet, A.; Parella, T.; Benet-Buchholz, J. *J. Am. Chem. Soc.* **2004**, *126*, 7798−7799.
(18) Shimazaki, Y.; Nagano, T.; Takesue, H.; Ye, B.; Tani, F.; Naruta, Y. *Angew. Chem., Int. Ed.* **2004**, *43*, 98−100.
(19) Zong, R. Z.; Thummel, R. P. *J. Am. Chem. Soc.* **2005**, *127*, 12802−12803.
(20) Baffert, C.; Romain, S.; Richardot, A.; Leprêtre, J.; Lefebvre, B.; Deronzier, A.; Collomb, M. *J. Am. Chem. Soc.* **2005**, *127*, 13694−13704.
(21) Narita, K.; Kuwabara, T.; Sone, K.; Shimizu, K.; Yagi, M. *J. Phys. Chem. B* **2006**, *110*, 23107−23114.
(22) Liu, F.; Cardolaccia, T.; Hornstein, B. J.; Schoonover, J. R.; Meyer, T. J. *J. Am. Chem. Soc.* **2007**, *129*, 2446−2447.
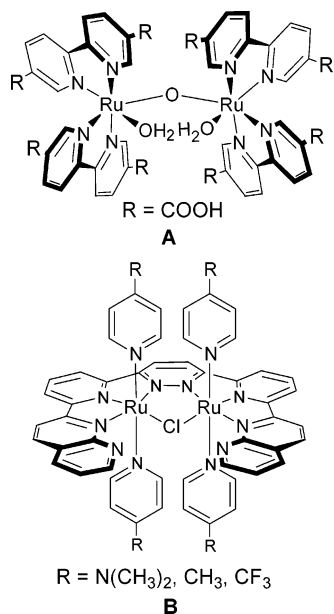
Figure 1. (A) Ruthenium dimer generated by Grätzel et al. in 1986,[10] and (B) three diruthenium complexes synthesized for water oxidation by Thummel in 2005.[19]

is the study performed by Grätzel and co-workers[10] in which a bis(aquo), bis(5,5′-dicarboxylated-2,2′-dipyridyl) ruthenium complex was oxidized to form an oxo-bridged binuclear catalyst for water oxidation, very similar to the mixed valence, blue ruthenium dimer originally developed by Meyer et al.[6] Not only is Grätzel's study one of the few to report dynamic monitoring of oxygen evolution, with a maximum O_2 evolution rate of 300 μL per hour, but they also report a turnover number of 75 when using Co(III) as an electron acceptor. More recently, Thummel and Zong described another class of diruthenium polypyridyl complexes that are active for water oxidation, with a reported maximum turnover number of 3200 for the electronically optimized case.[19] The active structures identified in the Grätzel and Thummel examples are depicted in A and B of Figure 1, respectively.

Notably, the primary polypyridyl ligand in Thummel's complex confines the two ruthenium molecules to a well-defined geometry, and electrochemical tunability may be possible by virtue of the substituents on the attached pyridine groups. Despite this system's enhanced catalytic activity, however, it also has its disadvantages, such as an increased complexity of design—especially the primary ligand's synthesis. In short, there is no existing synthetic catalyst for homogeneous water oxidation that is simultaneously simple, robust, and effective.

An alternative, cyclometalated iridium-based compound (structure shown in Figure 2) is presented as a synthetically accessible, robust, and efficient solution to some of the problems with existing catalysts. It is likewise demonstrated that the ligand structure of this species can be easily modified with various
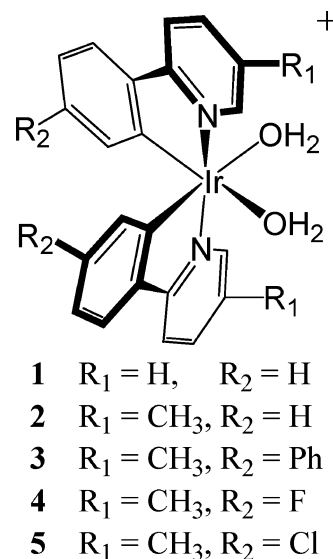
(23) Shafirovich, V. Y.; Shilov, A. E. *Kinet. Katal.* **1979**, *20*, 1156−1162.
(24) Harriman, A.; Richoux, M.; Christensen, P. A.; Mosseri, S.; Neta, P. *J. Chem. Soc., Faraday Trans. 1* **1987**, *83*, 3001−3014.
(25) Nahor, G. S.; Neta, P. *J. Phys. Chem.* **1988**, *92*, 4499−4504.
(26) Nahor, G. S.; Hapiot, P.; Neta, P.; Harriman, A. *J. Phys. Chem.* **1991**, *95*, 616−621.
(27) Hara, M.; Waraksa, C. C.; Lean, J. T.; Lewis, B. A.; Mallouk, T. E. *J. Phys. Chem. A* **2000**, *104*, 5275−5280.
(28) Chen, G.; Delafuente, D. A.; Sarangapani, S.; Mallouk, T. E. *Catal. Today* **2001**, *67*, 341−355.
(29) Hara, M.; Lean, J. T.; Mallouk, T. E. *Chem. Mater.* **2001**, *13*, 4668−4675.

1 R_1 = H, R_2 = H
2 R_1 = CH$_3$, R_2 = H
3 R_1 = CH$_3$, R_2 = Ph
4 R_1 = CH$_3$, R_2 = F
5 R_1 = CH$_3$, R_2 = Cl

Figure 2. Structure of the described oxidation catalyst, [Ir(5-R_1,4′-R_2,2-phenylpyridine)$_2$(OH$_2$)$_2$]$^+$.

electron withdrawing and electron-donating substituents, which serve to tune the HOMO energies of the respective iridium complexes, allowing us to control their oxidation potentials. The preparation of the parent (unsubstituted) species, first reported by Schmid et al. in 1994,[30] is straightforward and is herein proven versatile enough to generate aquo complexes with a wide range of cyclometalating ligands.

The kinetics of these water-oxidizing dark reactions are monitored via pressure transducers, which are mounted into the headspace of the reaction vessels. The strength of this approach is its simplicity, which renders analysis and quantization relatively unproblematic while providing a detailed picture of how the several reactions proceed, as well as mechanistic insights for the complicated chemistry that ensues.[31] Dynamic monitoring of these O_2-evolving reactions is crucial to understanding these systems and may aid ongoing efforts to pair such catalysts with appropriate water reduction analogues in a complete photosynthetic system.

Experimental Section

General. ^{1}H NMR spectra were recorded on a Bruker BioSpin Avance-500 MHz spectrometer at room temperature. Mass spectra (MS) were obtained using a Hewlett-Packard Electrospray (ESI) MS engine. Gas chromatography (GC) was performed with an argon carrier gas through a 12′ × 1/4″ column packed with 13×, 80/100 mesh molecular sieve (Alltech). This was incorporated into a Perkin-Elmer Model 3920 gas chromatograph with a thermal conductivity detector.

Materials. The cyclometalating ligands and cyclometalated iridium dimers were prepared as reported by Lowry et al.[32]

Synthesis of [Ir(ppy)$_2$(H$_2$O)$_2$]$^+$ and Analogues. The aquo complexes of cyclometalated iridium(III) dimers were prepared in a similar fashion to the synthesis employed by Schmid (see Scheme 1).[30] In place of Schmid's methanol/dichloromethane solvent system, a 9:1 mixture of ethanol/water was used to achieve the desired conversion in yields ranging from 44 to 76%. Specifically, the appropriate cyclometalated iridium chloride-bridged dimers were added to 9:1 mixtures of ethanol

(30) Schmid, B.; Garces, F. O.; Watts, R. J. *Inorg. Chem.* **1994**, *33*, 9−14.
(31) Tinker, L. L.; McDaniel, N. D.; Curtin, P. N.; Smith, C. K.; Ireland, M. J.; Bernhard, S. *Chem.−Eur. J.* **2007**, *13*, 8726−8732.
(32) Lowry, M. S.; Hudson, W. R.; Pascal, R. A.; Bernhard, S. *J. Am. Chem. Soc.* **2004**, *126*, 14129−14135.

Scheme 1. General Procedure for Cleaving the Chloride-Bridged Dimers to Procure the Aquo Compounds **1**−**5**
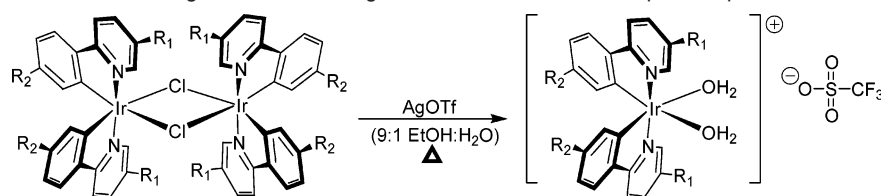
Table 1. Yields of Purified **1**−**5** Resulting from Cleavage of the Respective Chloride-Bridged Dimers with Silver Trifluoromethanesulfonate

Compound	Cyclometalating Ligand	Purified Yield
1		60%
2		65%
3		44%
4		76%
5		56%

(Pharmco, >99.5%) and water to make 0.01 M slurries. A total of 2.2 molar equiv of silver trifluoromethanesulfonate (Acros, >99%) was added to the slurries, after which the reaction mixtures were refluxed for 24 h. The product solutions were then concentrated under rotary evaporation, after which the product was extracted from the solids using dichloromethane (EM, 99.5%). After filtering the remaining silver salts, the solvent was once again removed under vacuum. Products were recrystallized by vapor diffusion from chloroform/pentane. Yields of purified products are reported in Table 1, whereas characterizations are described in the Supporting Information, including ^{1}H NMR, ^{13}C NMR, low-resolution MS, and elemental analysis.

Electrochemical Analyses. All cyclic voltammograms were recorded on a CH-Instruments Electrochemical Analyzer Model 600C. Studies in water were performed under neutral conditions using a 25 mm^2 indium tin oxide working electrode, a platinum coil counter electrode, and an Acumet SCE reference electrode. Studies in acetonitrile used a 1 mm^2 platinum working electrode, a platinum coil counter electrode, and a silver wire as a pseudo-reference electrode. Ferrocene (Aldrich) was then employed as an internal standard in acetonitrile, and its standard oxidation half-wave potential was taken to be 610 mV against the normal hydrogen electrode. Solutions for voltammetry were prepared with 0.1 M supporting electrolyte−sodium tetrafluoroborate (Aldrich, 98%) for water-based studies, and tetra-*n*-butylammonium hexafluorophosphate (Fluka, electrochemical grade) for analyses in acetonitrile. Solutions of **1**−**5** were prepared at 250 μM concentrations in either solvent, with the exception of **3**, which was only slightly soluble in water. Solutions were degassed with N_2 bubbling for 10 min before each voltammogram.

Dynamic Oxygen Evolution Measurements. All oxygen evolving reactions were contained by 40 mL EPA vials (VWR, Traceclean). The caps of these vials were modified to house pressure transducers (Omega PX-138-015D5V) for dynamic monitoring of the headspace pressure above each reaction in parallel. The caps were also equipped with septum seals, which facilitated degassing and reagent injections. All reactions were carried out under dark conditions at 25 °C, under argon headspace. The exact setup and procedure used to monitor these reactions is detailed in the Supporting Information. The output from the pressure transducers was scaled by GC analysis of the reactions' headspace.

Computational Studies. Hybrid density functional calculations (B3LYP/LANL2DZ) were performed using Gaussian 03.[33] Whereas the default parameter was used for gradient convergence, the threshold for wave function convergence was relaxed to CONVER=7, due to the presence of the heavy metal. Geometry optimizations for both singlet and doublet geometries were carried out under the constraint of C_2 symmetry.

Results and Discussion

Dioxygen-generating reactions were initiated by injecting aqueous solutions of cerium(IV) ammonium nitrate (CAN) into larger volumes of degassed aqueous solutions containing the aquo-iridium complex. Despite generation of O_2 from water and consequential discharge of H$^+$, the pH of these 10 mL reactions remains roughly constant at 0.7 ± 0.05 throughout the reactions' duration. Because the CAN was added as a standardized aqueous solution, the dominating species of ceric ion was presumably the aquo/hydroxo species,[5] and the constant pH is then explained by liberation of OH$^-$ upon reduction of Ce(IV) to Ce(III). Gas evolution was monitored by pressure transducer and later confirmed to be dioxygen by GC analysis. Control experiments involved allowing solutions of cerium(IV) to stand under identical reaction conditions as experienced by the catalyzed reactions and did not produce measurable oxygen during the typical 30-hour reaction window.

To ensure that the formed dioxygen originates from water rather than from the nitrate of CAN, ceric trifluoromethanesulfonate (OTf$^-$) was employed as an oxidant. It was found that the use of Ce(OTf)$_4$ in place of CAN also leads to oxygen production, confirming that water is being oxidized in these reactions. Notably, substituting Ce(OTf)$_4$ for CAN reduces the rate of the reaction by an order of magnitude. Likewise, adding an equivalent molar concentration (roughly 0.6 molar) of trifluoromethanesulfonic acid to aqueous CAN has a similar detrimental kinetic effect. Meanwhile, addition of an equivalent molar concentration of fluoroboric acid to aqueous CAN has negligible adverse effect on the rate of oxygen evolution, suggesting that the OTf$^-$ counterion somehow impedes the reaction. Additions of known ligating solvents such as acetonitrile and dimethylsulfoxide were found to similarly disrupt oxygen evolution. One final control was run in which the coordinating waters in **1** were replaced by an inert bipyridine moiety, the synthesis of which has been previously described.[32] To aqueous CAN was added the mock catalyst [Ir(ppy)$_2$(bpy)]$^+$, structure shown in Figure 3. No oxygen evolved from this mixture, suggesting that aquo coordination is essential. With this in mind, it is thus likely that free coordination sites on the iridium catalyst are a necessary condition for these reactions, precluding the use of strongly coordinating solvents or counterions in water oxidation reactions.

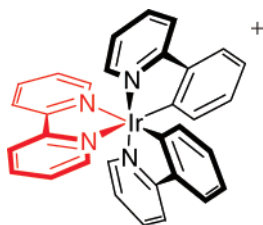(33) Frisch, M. J.; et al. *Gaussian 03*, revision C.02; Gaussian,Inc.: Wallingford, CT, 2004.

Figure 3. Structure of $[Ir(ppy)_2(bpy)]^+$, used as a surrogate catalyst in a control experiment to confirm the importance of free coordination sites.
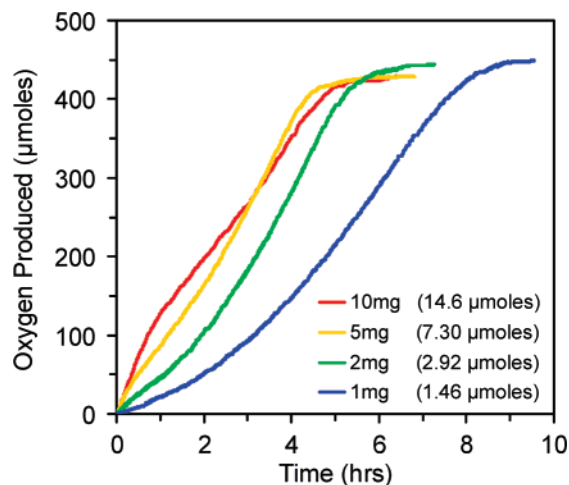

Figure 4. Pressure vs time curves for dioxygen evolution from solutions of **1** and cerium(IV). CAN (1720 μmol) was contained in these 10 mL aqueous reactions along with the specified amount of catalyst, bringing the theoretical maximum O_2 yield to 430 μmol for each experiment. At higher catalyst concentrations, the rate of reaction is observed to fall from its original rate, possibly due to competitive side reactions or an undesirable change in the catalyst's structure.

Rate Study. To better understand the mechanism of oxygen evolution, a series of parallel experiments were performed in which the reactant concentrations were varied. The headspace pressures above these reactions were monitored dynamically, and the GC-confirmed results are plotted in Figure 4. In each of the four experiments shown, 1.7 mmol of CAN from a stock solution were allowed to react with water in the presence of a varied amount of compound **1**. These reactions took place in a completely aqueous medium with a total solution volume of 10 mL. The reactions were allowed to proceed to completion, after which all evolved product volumes were within 4% of the theoretical maximum yield of 430 μmol of O_2.

One interesting phenomenon that appears in these traces is the unusual kinetic progression that occurs after a half hour of reaction. In particular, the shape of these kinetic traces can be organized into two regimes. The first section involves a constant, linear evolution of oxygen from the system. A comparison between these initial slopes, which reveals a non-first order dependence on catalyst concentration, can be found in the Supporting Information. The initial linear kinetic reaction proceeds for roughly 30 min before advancing to a parabolic curve. This parabola is then maintained until the cerium concentration dwindles, at which point the reaction tapers off and finishes. Whereas the shape of this second regime can be rationalized by assuming a general catalytic mechanism, the reaction's initiation and change of mechanism is more difficult to rationalize. With constant pH and roughly invariable [Ce(IV)] during the initial stages of the O_2 evolution process,
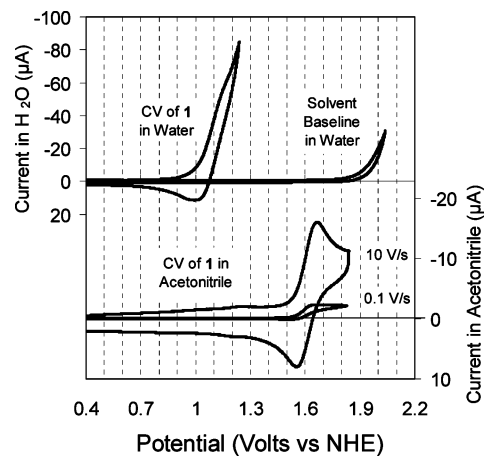

Figure 5. Cyclic voltammograms from a 250 μM solution of **1** in water, as well as the solvent baseline (top half). Scan rates in water were 0.1 V/s. The voltammograms on the bottom half are derived from a 250 μM solution of **1** in acetonitrile, at scan rates of 0.1 and 10 V/s. Supporting electrolyte was 100 mM $NaBF_4$ for water studies and 100 mM $N(n-Bu)_4PF_6$ for acetonitrile CVs.

it is clear that an *in situ* alteration in the catalyst must be responsible for the early changes in rate, suggesting that perhaps multiple active species are present throughout the course of the reaction. The specific nature of this change is currently under investigation.

Substitution on the Phenylpyridine. To explore the electrochemical tunability of this catalyst, several structurally altered derivatives were prepared for comparison to the parent complex. Static DFT calculations (B3LYP/LANL2DZ) aided in the ligand selection process for this demonstration. These calculations are discussed in further detail below. Ultimately, several complexes were chosen and prepared from substituted phenylpyridines and then analyzed for their electrochemical properties and ability to catalyze water oxidation. In particular, substitutions were made at the 4′ position on 5-methyl-2-phenylpyridine, and the resulting ligands were then used to form the respective cyclometalated iridium bis(aquo) complexes. These substituents ranged from electron-withdrawing groups like fluorine to electron-donating groups such as phenyl and are identified in Figure 2.

Cyclic voltammograms (CVs) in both water and acetonitrile were used to evaluate the oxidation potentials associated with these various species. For a number of reasons, aqueous voltammetry proved problematic with these compounds. Several working electrodes were employed, including gold, platinum, glassy carbon, and indium tin oxide surfaces. Most of these materials gave uninterpretable voltammograms due to surface adsorption of the catalyst onto the working electrode. However, ITO gave reasonably clean CVs under neutral aqueous conditions despite the surface adsorption problem.

Other complications included differing solubilities of **1**−**5** in water and solvent oxidation at reduced onset potentials, which tended to obscure the interesting Ir(III/IV) oxidation wave and invalidate comparisons of current between CVs. Shown in Figure 5 is the neutral, aqueous voltammogram of **1** as well as the solvent baseline. Also shown for comparison is the CV of **1** in acetonitrile on a separate axis. Markedly, the Ir(III/IV) wave is concealed for aqueous CVs by oxidation of the solvent, to the extent that deconvolution of the overlapping waves becomes problematic.
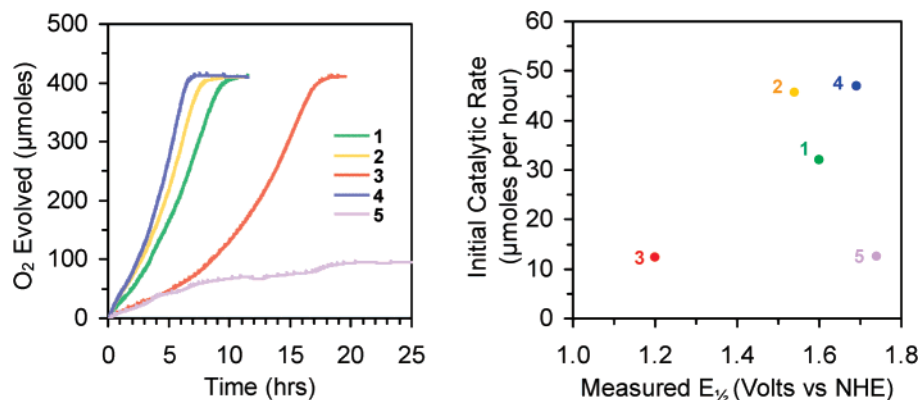
Figure 6. Depicted on the left is dynamic oxygen evolution from 10 mL aqueous solutions containing 3 μmol of the substituted catalysts and 1720 μmol of ceric ammonium nitrate. Though unbuffered except by the ceric ion, the pH of 0.7 ± 0.05 did not change appreciably during these reactions, presumably due to the sequential release of OH$^-$ upon reduction of Ce(IV) to Ce(III) and liberation of H$^+$ upon oxidation of water. On the right, the initial O$_2$-evolution rate from each of these curves (measured via linear least-squares regression of the oxygen generated during the first 45 min) is plotted against the oxidation potentials of these catalysts in CH$_3$CN, as determined by cyclic voltammetry.
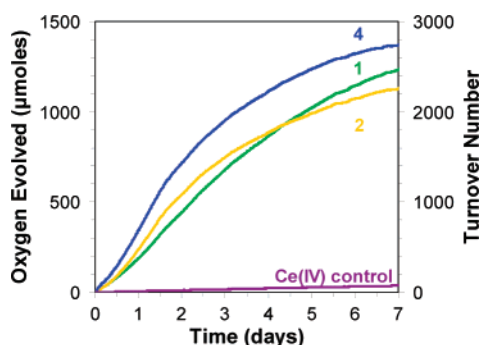

Figure 7. Week-long oxygen evolution is shown from 10 mL aqueous solutions containing 0.5 μmol of **1**, **2**, and **4** (the three most efficient catalysts) and an excessive 15 000 μmol of ceric ammonium nitrate, along with a catalyst-free control. The axis on the left measures micromoles of oxygen produced, whereas the axis on the right gives the conversion to turnover numbers. Analysis of the headspace gas revealed that 1240, 1140, and 1380 μmol of oxygen were generated by **1**, **2**, and **4**, respectively. These correspond respectively to maximum catalytic turnover numbers of 2490, 2270, and 2760.

Although this prevents a well-defined measurement of aqueous Ir(III/IV) oxidation potentials, there is nevertheless a relationship between aqueous oxidation onsets and the Ir(III/IV) waves measured in acetonitrile. The absolute potentials are shifted dramatically in going from one solvent to the other, due both to the altered polarity of the medium as well as to dynamic exchange between ancillary ligands and the solvent. However, the observed effect from adding electron donating/withdrawing substituents to the cyclometalated phenylpyridines is reasonably predictable upon considering the molecular orbitals of these complexes. The bottom of Figure 8 shows the calculated highest occupied molecular orbitals (HOMOs) for molecules **3** and **4**. No electron density resides on the ancillary ligands in these orbitals but rather is entirely located on the metal center and cyclometalated phenylpyridine ligands of the complexes. This agrees well with an earlier report by Goldsmith et al.[36] in which the HOMO of a similar complex (structure shown in Figure 3) is also shown to be roughly independent of the ancillary groups. It would not be unexpected, then, that the effect from phe-

nylpyridine substitution would be equivalent with either water or acetonitrile at the ancillary positions.

Negligible rate-related isotope effect was observed upon solvent substitution of D$_2$O for H$_2$O under constant pH 0.7 conditions (pH corrected for D$_2$O). This does not preclude the possibility that further processes involving proton-coupled charge transfers also occur during catalyzed water oxidation, but currently there is no evidence to suggest that this is the case for the rate-limiting step of these reactions.

Characterizations in acetonitrile were thus used to observe the relevant Ir(III/IV) electrochemical processes independently of the more complex steps that are necessarily involved when aqueous conditions are employed. Oxidation waves were observed for each of the five compounds, at potentials ranging from 1.20 to 1.74 V vs NHE. Two such waves are shown in the bottom half of Figure 5, performed on the parent complex **1** at sweep rates of 0.1 and 10 V/s. Notably, the shapes of these scans are quite different; the faster scan is more reversible than the slower scan, indicative of an EC mechanism. These results, as well as comparison to density functional theory predictions (discussed below), are summarized in Table 2.

These compounds were then tested for catalytic activity toward water oxidation by injecting 1.66 mmol of CAN into 300 μM solutions of the catalysts. In the case of the least soluble catalyst, **3**, the catalyst did not dissolve fully until addition of the oxidant. Oxygen was observed to evolve from all five of these reactions at varying rates. Their respective catalytic activities were quantified by calculating the maximum slope from the reactions' dynamic pressure traces (confirmed to be oxygen evolution). Both the original pressure traces as well as the initial catalytic rates, plotted against the catalysts' measured oxidation potentials, can be found in Figure 6. These initial rates were determined via linear least-squares regression of O$_2$ evolution from the first 45 min of the reaction. Compound **5** is observed to catalyze water oxidation at a comparatively reduced rate. This is believed to be a result of insufficient overpotential involved in the charge transfer between the Ir(III) center and the Ce(IV) ion, likely to be the initial step of water oxidation.

Stability of the Catalyst. To determine how many catalytic cycles the catalysts can endure, 0.5 μmol of **1**, **2**, and **4** were added to 15 000 μmol of aqueous CAN, after which the reaction mixture was put under vacuum and allowed to react for several

(34) Reiss, H.; Heller, A. *J. Phys. Chem.* **1985**, *89*, 4207−4213.
(35) Cossi, M.; Iozzi, M. F.; Marrani, A. G.; Lavecchia, T.; Galloni, P.; Zanoni, R.; Decker, F. *J. Phys. Chem. B* **2006**, *110*, 22961−22965.
(36) Goldsmith, J. I.; Hudson, W. R.; Lowry, M. S.; Anderson, T. H.; Bernhard, S. *J. Am. Chem. Soc.* **2005**, *127*, 7502−7510.
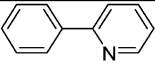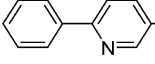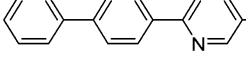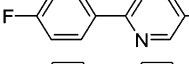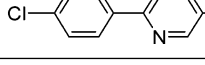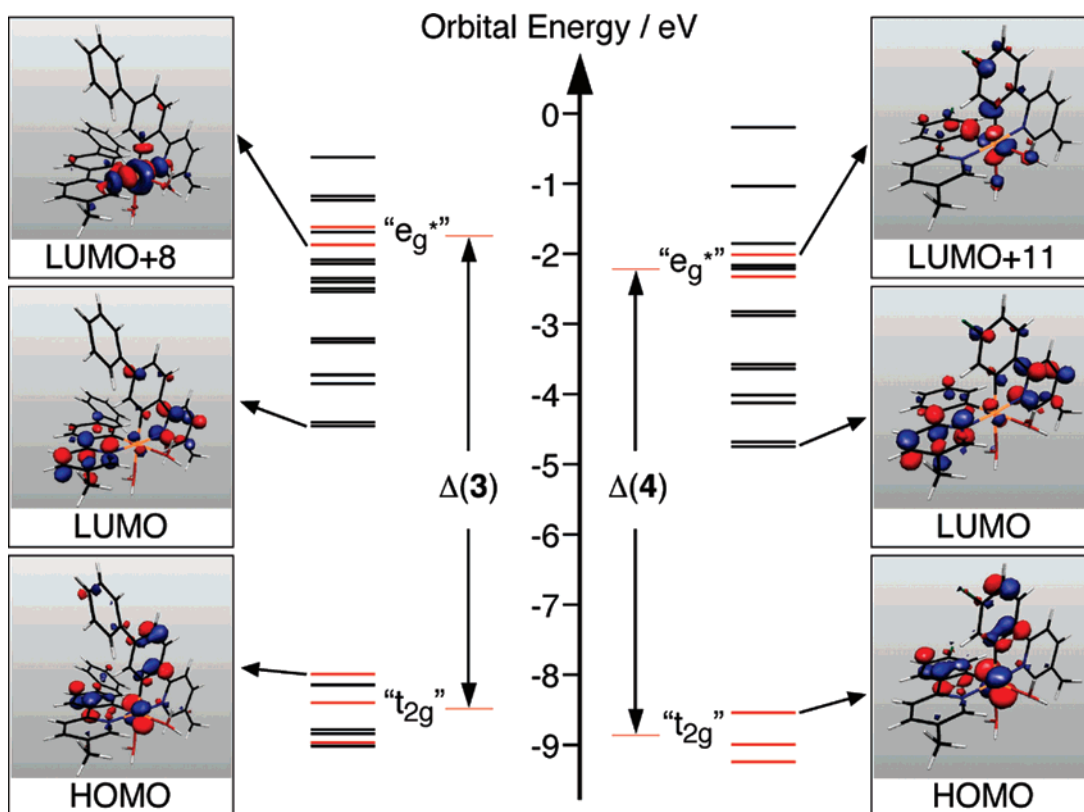
Figure 8. Frontier molecular orbital diagrams for compounds **3** and **4**, generated from DFT calculations, as well as rendered 95% surfaces of selected orbitals. Due to the mixed metal/π-system character of these orbitals, the addition of electron-donating or electron-withdrawing substituents (phenyl on the left, fluorine on the right) can be used to adjust the orbital energies of these compounds. Of particular interest is the ability to fine-tune the energy of the HOMO, which is strongly involved in the catalysis of water oxidation.

Table 2. Calculated and Measured Ionization Potentials for Removal of an Electron from Compounds **1**−**5**

Complex	Cyclometalating Ligand	Calc. E Method 1 (Volts)	Calc. E Method 2 (Volts)	Obs. E$_{1/2}$ vs NHE (Volts)
1		(1.60)*	(1.60)*	1.60
2		1.46	1.43	1.54
3		1.24	1.04	1.20
4		1.81	1.79	1.69
5		1.78	1.72	1.74

[a] All calculations were corrected by addition of a constant to bring the calculated potentials of **1** into agreement with its observed ionization potential.

days. Compounds **3** and **5** were omitted from this experiment due to their relatively slow reaction kinetics. The pressure traces of these reactions are shown in Figure 7. After a week, the reactions' headspaces were analyzed for oxygen by GC injection, and it was determined that 1240, 1140, and 1380 μmol of oxygen were generated by **1**, **2**, and **4**, respectively. This evolved product gas represents roughly one-third of the expected 3750 μmol for complete conversion. In addition, trace CO_2 was detected by MS, indicating that the catalyst's ligand sphere was at least partially oxidized by the end of the reaction. These

values correspond to catalytic turnover numbers of 2490 for **1**, 2270 for **2**, and 2760 for **4**.

Density Functional Theory Calculations. The electrochemical tunability of this catalyst architecture is a major advantage for its practical incorporation into photosynthetic schemes. This electronic flexibility would not be possible if the highest occupied molecular orbitals (HOMOs) of these complexes did not demonstrate mixed ligand/metal character, that is, the cyclometalating nature of the ppy ligands allows them to interact strongly with the metal center, forming frontier molecular
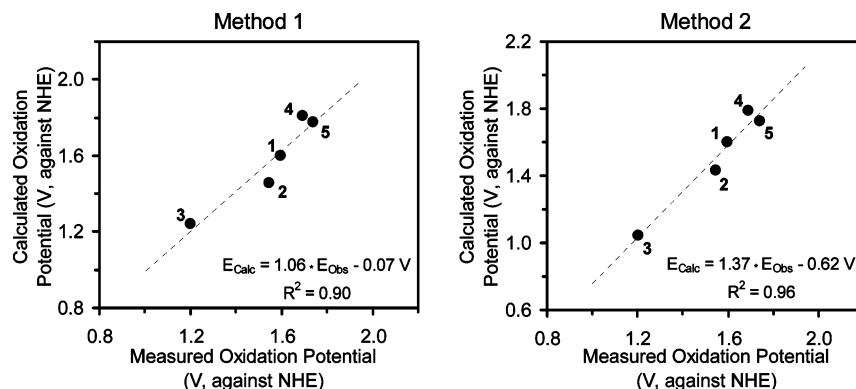
Figure 9. Static DFT calculations were used as a predictive tool for determining an appropriate set of cyclometalating ligands for an electronic tunability demonstration. Complexes generated from the chosen ligands exhibit properties that correlate well with their predicted values. Two methods were used to make these predictions: in method 1 (left), the geometry-optimized HOMO energies of the various complexes were calculated and used to estimate their ionization potentials, disregarding any electronic or geometric rearrangements that might occur in the oxidized species. In method 2 (right), both the ground state singlet and oxidized doublet species were geometrically/electronically optimized, and the difference between their predicted absolute energies was used as an estimation of their ionization potentials.

orbitals with the iridium that incorporate both the metal's d-orbitals and the ppy's π-system. In general, by adding substituents to the phenyl ring of the ppy, the ligands become either more electron-withdrawing or electron-donating, thereby respectively stabilizing or destabilizing the HOMO. Shown in Figure 8 are the molecular orbital diagrams for compounds **3** (left) and **4** (right), whose HOMOs are known by cyclic voltammetry to have a ~0.5 V difference in potential. These MO diagrams, as well as the 95% surfaces depicted for selected MOs, were generated through static density functional theory calculations for the geometry-optimized singlet ground states of each species. As shown in the figure, their predicted ligand-field splitting potentials are very similar, but the mixed orbitals of **4** are expected to be lower in energy than those of **3**, due to electronic stabilization from the withdrawing fluorine substituent.

Two computational methods were used to extract meaningful predictions from these calculations. In particular, "method 1" and "method 2," described below, were used to arrive at expected relative ionization potentials for the complexes of interest. Both were found to give accurate predictions for this observable. In each of the offered methods, referencing to standardized electrodes was achieved by shifting all predicted values by a common constant, as is the general protocol for these comparisons.[34,35] The results of these calculations are summarized both in Table 2 and Figure 9.

Method 1: As a rough but efficient predictor of ionization potentials, the ground state, singlet geometries of the desired complexes were optimized, and the energies of their HOMOs were compared. To reference these values to the normal hydrogen electrode, a common 6.96 V constant was subtracted from the free ions' calculated HOMO energies. The results are plotted in Figure 9 (left side) against the voltammetrically observed ionization potentials. Notably, a linear least-squares regression through the data gives a respectable Pearson factor of 0.90, with a slope of roughly unity.

Method 2: In a more extensive approach, the ionization potentials were estimated by taking the difference in total calculated energy between the geometry-optimized ground state and first oxidized state of the compounds. Specifically, geometry optimization was performed on both the singly charged, lowest energy singlet configuration, as well as the doubly charged, oxidized doublet configuration, prior to energetic comparison.

To reference the predictions to NHE, a common 7.92 V constant was subtracted from the raw energy differences of the free ions. The results of this calculation are likewise plotted against the measured potentials in Figure 9 (right side). The Pearson factor for these data is superior to that generated using Method 1, but the slope of the regression line is farther from unity. In general, one would expect Method 2 to better predict the ionization potentials of a given structure, though it is also a lengthier calculation.

Conclusions

This report details the homogeneous, chemically driven oxidation of water by a class of easily synthesized cyclometalated iridium(III) aquo complexes. These compounds have four notable selling points as water-oxidation catalysts: First, their design is quite simple, which makes their synthesis comparatively economical. Second, their ligand framework is bound by a strong carbon–iridium bond, making them exceptionally robust under typical reaction conditions. Third, they are water soluble at various pH, eliminating the need for mixed solvent systems. Fourth, their HOMO energies are herein shown to be highly tunable through substitution on the cyclometalated ligands, which allows us to selectively tune their oxidative potentials. As previously shown, the HOMO and LUMO energy levels of similar heteroleptic polypyridyl iridium(III) luminophores are likewise highly tunable through ligand design.[32,36,37] In particular, it is now known that the cyclometalating ligands in these systems play a large role in determining the HOMO energy of the complexes. Thus, the ability to tune the electronics of both the catalyst and the photosensitizer may facilitate ongoing efforts to couple these two species in photodriven half reactions, or even full water-splitting schemes.

Supporting Information Available: The detailed protocol for dynamic monitoring and quantification of oxygen evolution, as well as the structural characterizations of the compounds of

(37) Lowry, M. S.; Goldsmith, J. I.; Slinker, J. D.; Rohl, R.; Pascal, R. A.; Malliaras, G. G.; Bernhard, S. *Chem. Mater.* **2005**, *17*, 5712−5719.

interest (inlcuding ^{1}H NMR, ^{13}C NMR, electrospray ionization MS, and elemental analyses) are provided. Also included is a detailed comparison between the initial rates of the reactions shown in Figure 4 and the complete citation for ref 33.

This material is available free of charge via the Internet at http://pubs.acs.org.